

1 **Electrochemical sensing with nanopores**

2

3 István Makra,^a Róbert E. Gyurcsányi,^{b,*}

4 ^aDepartment of Inorganic and Analytical Chemistry, Budapest University of Technology and
5 Economics

6 Szent Gellért tér 4, H-1111 Budapest, Hungary

7 ^bMTA-BME “Lendület” Chemical Nanosensors Research Group, Department of Inorganic and
8 Analytical Chemistry, Budapest University of Technology and Economics

9 Szent Gellért tér 4, H-1111 Budapest, Hungary

10 E-mail: robertgy@mail.bme.hu

11

12 **Abstract**

13

14 We discuss representative electrochemical nanopore sensing strategies, highlighting their
15 underlying theoretical principles, and limitations.

16

17 **Keywords**

18 Nanopore sensor, resistive pulse sensing, Coulter counting, stochastic sensing

19

20 **1. Introduction**

21

22 The use of nanopores for chemical sensing generally narrows down to nanoporous
23 membranes with straight-through pores of uniform size distribution and ultimately to single
24 nanopore membranes. To understand what makes nanopores so unique in terms of their use for
25 chemical sensing we must consider the extremely small volume defined by their interior. Thus
26 species translocating or residing within a nanopore can effectively change the physical-
27 chemical properties of the nanopore interior (e.g., conductance [1, 2] or refractive index [3]),
28 which can be detected in a label-free manner. By having a single nanopore with a volume
29 comparable to that of the targeted species, detection of single species becomes feasible. The
30 use of nanopores for electrochemical sensing originates in the Coulter counter, best known for
31 blood-cell counting in hematology [4]. However, the instrumentation and implementation of
32 biological nanopores additionally benefited from studies on biological ion channels [5, 6].
33 Conventional Coulter counters use a single cylindrical pore to count and size particles
34 suspended in an electrolyte. Pulsewise changes in the pore conductance are detected as

35 insulating particles passing through replace their own volume of highly conducting electrolyte
36 (Fig. 1). The analytical information from a resistive pulse sensing (RPS) measurement is the
37 pulse height (indicative of the volume of the target), pulse frequency (proportional to target
38 concentration) and pulse length (depends on the mean translocation velocity and relative lengths
39 of the pore and the target species).

40

41 A major strength of the method is the ability to determine particle concentration in a
42 calibration-less manner by relating the number of pulses to the known volume of suspension
43 flown through the pore. The classical apparatus detect species of ca. 2 to 60 % of the pore
44 diameter [8] and since the smallest pore diameter is 10 μm the lower size limit of the assessable
45 species is a few hundred nanometers. The reduction of the pore size is an obvious way to extend
46 the applicability of the Coulter principle to species with characteristic dimensions in the lower
47 nanometer range, e.g., nanoparticles of synthetic or biological origin, and macromolecules.
48 However, such a scaling down proved to involve essential changes compared to micropores and
49 to enable new detection methodologies.

50

51 **2. Resistive pulse sensing with single nanopores**

52

53 While in case of micropores the dominant transport form is the pressure driven flow through
54 the pore, the volume flow rates established through nanopores are orders of magnitude smaller
55 and therefore less efficient. Additionally, in case of charged species or pores the electrophoretic
56 or electroosmotic contributions, respectively, should be considered. In practice, the transport
57 through nanopores occurs through concurrent diffusive, hydrodynamic, electrophoretic, and
58 electroosmotic mechanisms resulting in a mean translocation velocity. Generally, for larger
59 diameter pores ($d > 10$ nm) the dominant mechanism is the hydrodynamic transport owing to its
60 quadratic dependence on the pore diameter. For $d < 10$ nm electrophoresis and electroosmosis
61 dominate; with relative contributions depending on the surface charge density of the pore and
62 the translocating species. Diffusive transport scales with $1/d$ and becomes comparable to
63 electrophoresis only for $d < 1$ nm,[9] because diffusion of smaller particles is faster while
64 electrophoresis is practically independent of the pore diameter. Thus, a calibration-less
65 concentration determination is challenging with nanopores unless the hydrodynamic transport
66 prevails. In case of hydrodynamic transport while difficult to determine the minute volume flow
67 rates experimentally, they can be calculated if the pore geometry is known [10]:

68

$$Q = \frac{3\pi P}{8\eta l} \frac{d_b - d_t}{d_b^3 - d_t^3} d_b^3 d_t^3$$

69 where, P is the applied pressure η is the electrolyte dynamic viscosity, l is the pore length, d_b
70 and d_t are the base and tip diameters of the conical pore geometry, respectively. Thus the pore
71 geometry, generally cylindrical or conical, clearly plays an important role in nanopore sensing,
72 by determining the electrical resistance, the shape of the current pulses and the overall
73 sensitivity of the detection. The uniform cross-section of cylindrical pores results in square
74 wave pulses, while the growing cross-section in conical pores causes an asymmetric triangle-
75 like pulse shape [11] (Fig.1).

76

77 2.1. Electrical resistance of nanopores

78 The general expression of the pore resistance assumes a conical pore geometry (in fact
79 truncated cone) and homogeneous conductivity (valid at high ionic strengths):

80

$$R_p = \frac{1}{\sigma} \int_{x=0}^l \frac{1}{A(x)} dx = \frac{4l}{\pi d_t d_b \sigma}$$

81 where σ is the electrolyte conductivity, x is the coordinate along the centerline, $A(x)$ is the
82 cross-section at position x , d_b , d_t , and α are the base and tip diameters of the truncated cone,
83 and the half-cone angle, respectively ($d_b = d_t + 2 \tan(\alpha)l$).

84 Since the electric field lines gradually converge into the pore orifice, the changing cross-
85 sections of the ion flux can contribute significantly to the overall pore resistance. This additive
86 component is called the access resistance (R_a) derived first by Hall [12]:

87

$$R_a = \frac{1}{2d\sigma}$$

88 Considering R_a at both openings the total resistance of a conical pore is

89

$$R = \frac{1}{\sigma} \left(\frac{4l}{\pi d_t d_b} + \frac{1}{2d_t} + \frac{1}{2d_b} \right)$$

90 while for cylindrical pores ($d_t = d_b = d$), $R = \frac{4}{\sigma d \pi} \left(\frac{l}{d} + \frac{\pi}{4} \right)$. The total resistance deviates

91 with only 3% from values simulated at $l/d=5$ using Nernst-Planck/Poisson equation, as
92 opposed to 20% when the access resistance is unaccounted. The discrepancy is even higher
93 for pores with lower l/d ratio.

94

95

96

97 *2.2.Theoretical models to estimate pulse amplitudes*

98 During particle translocation the maximal resistance change determines the current pulse
99 amplitude or peak height for “triangular” shaped pulses. For simplified models, such as
100 considering uncharged pores, insulating spherical targets and translocation along the pore axis
101 the pulse amplitude can be calculated analytically. However, in many practical cases one or
102 more of the above assumptions is not valid and therefore numerical solutions of coupled
103 Poisson, Nernst-Planck and Navier-Stokes differential equations [13] are used to provide the
104 pulse amplitudes (and shapes), but at largely increased computation times.

105

106 *2.2.1. Cylindrical pores*

107 There are four main models to calculate the pulse amplitude for cylindrical pores, each with
108 different validity region depending on the relative particle size (d_{part}/d) (Fig. 2.) [14]. The
109 earliest model uses the equation derived by Maxwell for the effective resistivity of a suspension
110 of insulating particles [15]. The model introduced by Gregg and Steidley treats the pore as an
111 ideal conductor containing an insulating sphere. Homogenous electric field is assumed although
112 the electric field lines distort around the particle resulting in an unaccounted resistive
113 contribution. Therefore, the model approximates the pulse amplitude from below [16]. Deblois
114 et al. assumed a “bulging” pore shape that follows the distorted electric field lines around the
115 particle. This modified shape enables to calculate the particle containing pore resistance exactly,
116 but underestimates the resistance of the empty pore by neglecting the electric field
117 inhomogeneity near the bulge. Therefore, this model provides an upper limit for the pulse
118 amplitude [1].

119 Anderson and Quinn [17] developed the fourth model on the analogy to the numerical
120 calculations of Smythe, who investigated the hydrodynamic resistance change in a cylinder
121 caused by a sphere [18]. This model has the broadest validity covering the whole practically
122 relevant particle size range (up to $d_{part} / d = 0.9$).

123
$$\frac{\Delta R}{R} \Big|_{Smythe} = \frac{1}{\left[\left(d / d_{part} \right)^3 - 0.8 \right] (l / d + \pi / 4)}$$

124
$$\frac{\Delta I}{I} = \frac{-\Delta R / R}{\Delta R / R + 1}$$

125 where ΔR is the resistance change, R is the resistance of the empty pore with access terms, ΔI
126 is the pulse amplitude.

127

128 2.2.2. Conical pores

129 To date there is no simple analytical expression for calculation of RPS pulse amplitudes in
130 conical pores. The main approaches to relate the pulse amplitude to the particle size and pore
131 geometry include:

- 132 -approximation of the very end of the conical pore with a cylinder [19],
- 133 -applying the model developed by Gregg to a conical pore geometry [20],
- 134 -calibration with nanoparticles of known size and assuming that the pulse height is
135 approximately proportional to the particle volume [21].

136 These approaches are valid only at sufficiently high electrolyte concentrations because the
137 number of counter ions shielding the surface charge of the nanopore [22] or the analyte [23, 24]
138 should remain negligible in the pore interior with respect to the free ions of the electrolyte. The
139 resistance calculations also assume continuum media which is valid until the smallest
140 dimension of the pore is larger than 10 nm [25].

141

142 2.3. Noise during RPS measurements

143 After electrical shielding RPS measurements are affected by ΔI_T thermal noise stemming from
144 the thermal motion of charge carriers, the ΔI_D dielectric noise due to the energy dissipated by
145 the dielectric pore substrate, the ΔI_A amplifier noise generated by the headstage and the ΔI_F
146 flicker (or 1/f) noise, arising only when voltage is applied. [26, 27] These noise components are
147 independent and the total noise level is:

$$148 \quad \Delta I_{total} = \sqrt{\Delta I_T^2 + \Delta I_D^2 + \Delta I_A^2 + \Delta I_F^2}$$

149 The noise is attenuated by electrical shielding, analog/digital noise filtering and using low-
150 noise/low-capacitance materials for the nanopore membrane. The bandwidth of the
151 measurement can influence both the noise level and the shape of the current pulse. While a high
152 bandwidth increases the noise, a bandwidth lower than the highest frequency component of a
153 translocation pulse results in signal attenuation/distortion. Considering this trade-off the cut-off
154 frequency during RPS experiments is generally 10 kHz. Commonly, thermal noise dominates
155 when R is less than ca. 10 M Ω , while at ca. 100 M Ω resistance and 20 kHz cut-off frequency
156 the amplifier and dielectric noise also become comparable. Above 100 M Ω pore resistance

157 usually amplifier or dielectric noise sets the total noise level while the flicker noise is typically
158 not dominant because of signal filtering.

159

160 *2.4. RPS for selective detection*

161 Solely size and shape information are not sufficient to identify target species in a complex
162 matrix. Therefore, selective receptors either immobilized to the nanopore environment or added
163 to the sample solution have been used to induce target-specific changes in the RPS signal.
164 Selective receptor is added to the sample generally to increase the size of the target species and
165 consequently the pulse amplitudes. This principle is illustrated in Fig. 3A through selective
166 detection of viruses by adding capsid-binding antibodies into the sample [28]. An alternative
167 approach is to monitor the translocation of a receptor the conformation (size) of which is altered
168 upon binding the target species. A relevant example is the detection of cocaine through the
169 blocked translocation of the cocaine-specific aptamer, which suffers a conformation change
170 upon cocaine binding that prohibits its translocation through the pore [23]. Using solid-state
171 nanopores through which double-stranded DNA strands translocate, but not their complexes
172 with restriction enzymes, allowed the identification of single-nucleotide polymorphism by
173 detecting the increase in the threshold voltage, i.e., the minimum voltage required to drive the
174 DNA strands through the nanopore by releasing the restriction enzyme[29].

175 In the simple case of having immobilized receptors that on the time scale of the analysis
176 bind their target reversibly with 1:1 stoichiometry the pulse duration can be related to the
177 dissociation rate constant (k_{off}) of the analyte-receptor complex:

$$178 \quad \Delta t = \frac{1}{k_{off}}$$

179 The mean time between successive binding events is a function of both the concentration and
180 the association rate constant (k_{on}) [30]:

$$181 \quad \Delta t_{on} = 1/k_{on} c .$$

182 Thus, for selective stochastic sensing low affinity receptors can be used bot for
183 quantitative determination of the target as well as to determine the kinetics of single molecule
184 binding events [31, 32]. In case of “irreversible” target binding permanent blockage events are
185 observed [32, 33], which can be used for a “Yes-No” type identification of a given species.
186 Quantitative detection is also feasible by measuring the mean time elapsed until the target binds
187 to the receptor, which is inversely proportional to its concentration [33]. In the case when the
188 single nanopore possess multiple binding sites (Fig. 3B), characteristic to receptor

189 functionalized solid-state nanopores, the time elapsed between the first and second binding can
 190 be used as a more convenient modality for quantitative analysis [34]. Multipore membranes can
 191 be also used for quantitative sensing, in which case a cumulated change of the membrane
 192 resistance is detected, without the possibility to differentiate single binding events [35].

193

194 2.5. Detection limit of RPS

195 While RPS has single species detection capability, as the signal is due to individual species
 196 translocating through the nanopore, the detection limit is in fact determined by the target
 197 throughput. At low concentrations the probability of a species encountering the pore becomes
 198 very small; the limiting situation being the undirected, Brownian motion of a single particle in

199 a volume V , that requires a mean encounter time of $t_e = \frac{V}{2Dd}$ (D is the diffusion coefficient of

200 the target) [36]. Thus, in RPS the translocation frequency decreases with the analyte
 201 concentration, but for statistical analysis there is an f_{event}^{min} minimal frequency that results in a
 202 practical measurement time (e.g. 100 pulses in 10 minutes). It is possible to increase the event
 203 frequency (e.g. by applying hydrostatic pressure), but at the expense of a higher translocation
 204 velocity, that shortens the duration of the current pulse. Shorter pulses than the electronic filter
 205 rise time τ_{rise} , will be attenuated and thus useless for analyte sizing. The salt gradient method
 206 used by Wanunu et al. is to date the only approach to simultaneously boost translocation
 207 throughput and increase translocation time [37].

208 Assuming that the flux of target species is the constant through every cross-section of
 209 the analyte flow, c_{min} can be introduced as the minimal concentration, which is measurable
 210 without significant attenuation of the pulse amplitude:

$$211 \quad c^{min} = \frac{1.36}{d^2 \pi l_{rise} N_A} \frac{f_{event}^{min}}{f_c^{max}}$$

212 where d is the diameter of the pore orifice (the tip diameter for conical pores), N_A is the
 213 Avogadro-constant, f_c^{max} is the maximal cut-off frequency where the analyte is still detectable
 214 irrespective of the current noise. The parameter l_{rise} is the distance between the analyte
 215 positions where the current pulse starts to deviate from the baseline and where it starts to deviate
 216 from the peak value (Fig. 4). The approximations $l_{rise}^{cyl} = d_{part} / 2 + l$ for cylindrical,

217 $I_{rise}^{cone} = \frac{d_{part}}{2}$ for conical geometries were used with $\tau_{rise} = \frac{0.34}{f_c}$ as typical in RPS

218 measurements [7].

219 Larger pores require lower analyte concentration because the detection limit scales inversely
220 with the pore volume (cylindrical pores) or with the third power of the tip diameter (conical
221 pores). According to Fig. 4 the detection limit of cylindrical pores is always lower than of
222 conical pores at equal pore/tip diameters. Generally, this is not true because conical pores are
223 more sensitive than cylindrical pores that enables to use a wider orifice for the same particle
224 size.

225

226 **3. Potentiometric sensing**

227 Owing to the small diameters of nanopores the chemical-physical properties of the surface can
228 selectively alter the transpore flux of ions through the nanopore (Fig. 3C). An early
229 potentiometric study showed that membranes with charged nanopores rejected ions of the same
230 charge sign and transported those of opposite charge [38]. The potentiometric response of such
231 permselective nanopores can be described well by using the Nernst-Planck/Poisson equations
232 [39]. Further increasing the transport selectivity of the nanopores by restricting it to a single ion
233 is possible by using a selective complexing agent (Ag^+ ionophore) and a hydrophobic
234 compound grafted to surface of the nanopore, in addition to ion-exchanger sites. Simple
235 potentiometric measurement of the membrane potential resulted in Ag^+ -selective electrodes
236 with nanomolar detection limit and selectivity coefficients exceeding six order of magnitudes
237 for common ions [40].

238

239 **4. Acknowledgement**

240 We thank for the support of the Lendület program of the Hungarian Academy of Sciences and
241 TÁMOP-4.2.1/B-09/1/ KMR-2010-0002.

242

243 **5. References**

244 [1] R.W. Deblois, C.P. Bean, Rev. Sci. Instrum., 41 (1970) 909-916.

245 [2] J.J. Kasianowicz, E. Brandin, D. Branton, D.W. Deamer, PNAS, 93 (1996) 13770-13773.

246 [3] V.S.-Y. Lin, K. Motesharei, K.-P.S. Dancil, M.J. Sailor, M.R. Ghadiri, Science, 278
247 (1997) 840-843.

248 [4] W.H. Coulter, in: U. Patent (Ed.), United States, 1953, Ch. 2656508.

- 249 [5] S.B. Hladky, D.A. Haydon, *Nature*, 225 (1970) 451-453.
- 250 [6] E. Neher, B. Sakmann, *Nature*, 260 (1976) 799-802.
- 251 [7] D. Pedone, M. Firnkes, U. Rant, *Anal. Chem.*, 81 (2009) 9689-9694.
- 252 [8] H. Bayley, C.R. Martin, *Chem. Rev.*, 100 (2000) 2575-2594.
- 253 [9] G.R. Willmott, M.G. Fisk, J. Eldridge, *Biomicrofluidics*, 7 (2013) 064106.
- 254 [10] G.S. Roberts, S. Yu, Q. Zeng, L.C.L. Chan, W. Anderson, A.H. Colby, M.W. Grinstaff,
255 S. Reid, R. Vogel, *Biosens. Bioelectron.*, 31 (2012) 17-25.
- 256 [11] G.R. Willmott, B.E.T. Parry, *J. Appl. Phys.*, 109 (2011) 094307.
- 257 [12] J.E. Hall, *J Gen Physiol*, 66 (1975) 531-532.
- 258 [13] S. Tseng, C.-Y. Lin, J.-P. Hsu, L.-H. Yeh, *Langmuir*, 29 (2013) 2446-2454.
- 259 [14] Z. Qin, J. Zhe, G.-X. Wang, *Meas. Sci. Technol.*, 22 (2011) 045804.
- 260 [15] J. Maxwell, Clarendon Press, Oxford, 1873.
- 261 [16] E. Gregg, *Biophys. J.*, 5 (1965) 393-405.
- 262 [17] J.L. Anderson, J.A. Quinn, *Rev. Sci. Instrum.*, 42 (1971) 1257-1258.
- 263 [18] W.R. Smythe, *Phys. Fluids*, 7 (1964) 633-638.
- 264 [19] D. Kozak, W. Anderson, M. Grevett, M. Trau, *J. Phys. Chem. C*, 116 (2012) 8554-8561.
- 265 [20] Y. Wang, K. Kececi, M.V. Mirkin, V. Mani, N. Sardesai, J.F. Rusling, *Chem. Sci.*, 4
266 (2013) 655-663.
- 267 [21] R. Vogel, G. Willmott, D. Kozak, G.S. Roberts, W. Anderson, L. Groenewegen, B.
268 Glossop, A. Barnett, A. Turner, M. Trau, *Anal. Chem.*, 83 (2011) 3499-3506.
- 269 [22] R.M.M. Smeets, U.F. Keyser, D. Krapf, M.-Y. Wu, N.H. Dekker, C. Dekker, *Nano Lett.*,
270 6 (2006) 89-95.
- 271 [23] J. Menestrina, C. Yang, M. Schiel, I.V. Vlassioux, Z.S. Siwy, *J. Phys. Chem. C*, 118
272 (2014) 2391-2398.
- 273 [24] W. Lan, C. Kubeil, J. Xiong, A. Bund, H.S. White, *J. Phys. Chem. C*, 118 (2014) 2726-
274 2734.
- 275 [25] W. Sparreboom, A. van den Berg, J.C.T. Eijkel, *New J. Phys.*, 12 (2010) 015004.
- 276 [26] J.D. Uram, K. Ke, M. Mayer, *ACS Nano*, 2 (2008) 857-872.
- 277 [27] R.M.M. Smeets, U.F. Keyser, N.H. Dekker, C. Dekker, *PNAS*, 105 (2008) 417-421.
- 278 [28] J.D. Uram, K. Ke, A.J. Hunt, M. Mayer, *Angew.Chem.Int.Ed.*, 45 (2006) 2281-2285.
- 279 [29] Q. Zhao, G. Sigalov, V. Dimitrov, B. Dorvel, U. Mirsaidov, S. Sligar, A. Aksimentiev,
280 G. Timp, *Nano Lett.*, 7 (2007) 1680-1685.
- 281 [30] H. Bayley, P.S. Cremer, *Nature*, 413 (2001) 226-230.
- 282 [31] S. Howorka, L. Movileanu, O. Braha, H. Bayley, *PNAS*, 98 (2001) 12996-13001.

- 283 [32] L. Movileanu, S. Howorka, O. Braha, H. Bayley, *Nat. Biotechnol.*, 18 (2000) 1091-1095.
- 284 [33] Z. Siwy, L. Trofin, P. Kohli, L.A. Baker, C. Trautmann, C.R. Martin, *J. Am. Chem. Soc.*,
- 285 127 (2005) 5000-5001.
- 286 [34] S. Ding, C.L. Gao, L.Q. Gu, *Anal. Chem.*, 81 (2009) 6649-6655.
- 287 [35] G. Jágorszki, R.E. Gyurcsányi, L. Höfler, E. Pretsch, *Nano Lett.*, 7 (2007) 1609-1612.
- 288 [36] L. Höfler, R.E. Gyurcsányi, *Anal. Chim. Acta*, 722 (2012) 119-126.
- 289 [37] M. Wanunu, W. Morrison, Y. Rabin, A.Y. Grosberg, A. Meller, *Nat. Nanotechnology*, 5
- 290 (2010) 160-165.
- 291 [38] M. Nishizawa, V.P. Menon, C.R. Martin, *Science*, 268 (1995) 700-702.
- 292 [39] I. Makra, G. Jágorszki, I. Bitter, R.E. Gyurcsányi, *Electrochim. Acta*, 73 (2012) 70-77.
- 293 [40] G. Jágorszki, Á. Takács, I. Bitter, R.E. Gyurcsányi, *Angew. Chem. Int. Ed.*, 50 (2011)
- 294 1656-1659.

295 **Figure captions**

296

297 Fig. 1. Schematics of a single nanopore sensor (left) and typical current responses for cylindrical
298 and conical pores (right). The ionic current through the nanopore is maintained by applying a
299 transmembrane voltage between two Ag/AgCl electrodes. The full width at half maximum
300 (fwhm) is a measure of the pulse duration while ΔI of the pulse amplitude [7].

301

302 Fig. 2. Relative current changes calculated with different models in a cylindrical pore with
303 $l/d=20$ as a function of the relative particle size. Regions in brackets indicate approximate
304 validity range of the models.

305

306 Fig. 3. Schematics of nanopore sensing methods and resulting signals. (A) RPS measurement
307 with a selective reagent added to the sample, (B) analyte binding by a functionalized nanopore,
308 (C) nanopore-based ion-selective membrane.

309

310 Fig. 4. Detection limit for particle sizing as function of pore diameter for a conical pore and
311 cylindrical pores with various lengths ($d_{part} / d = 0.5; f_c^{max} = 10 \text{ kHz}$).

Figure 1

[Click here to download high resolution image](#)

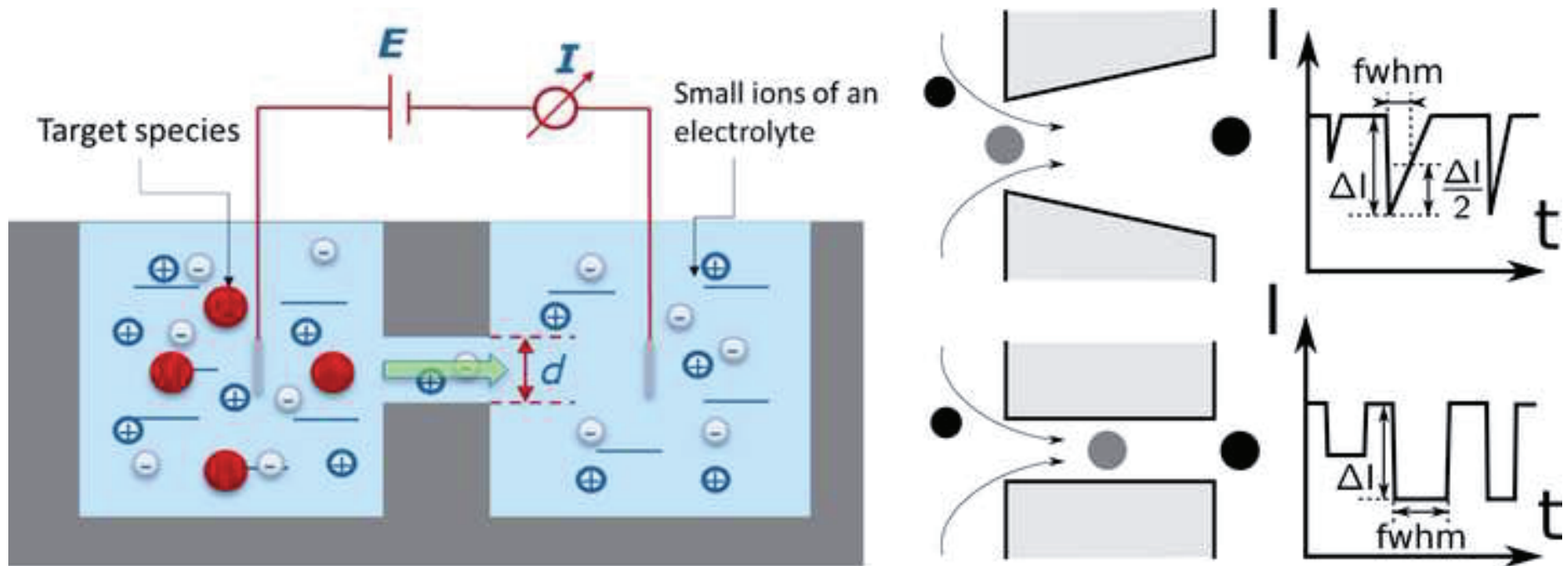


Figure 2

[Click here to download high resolution image](#)

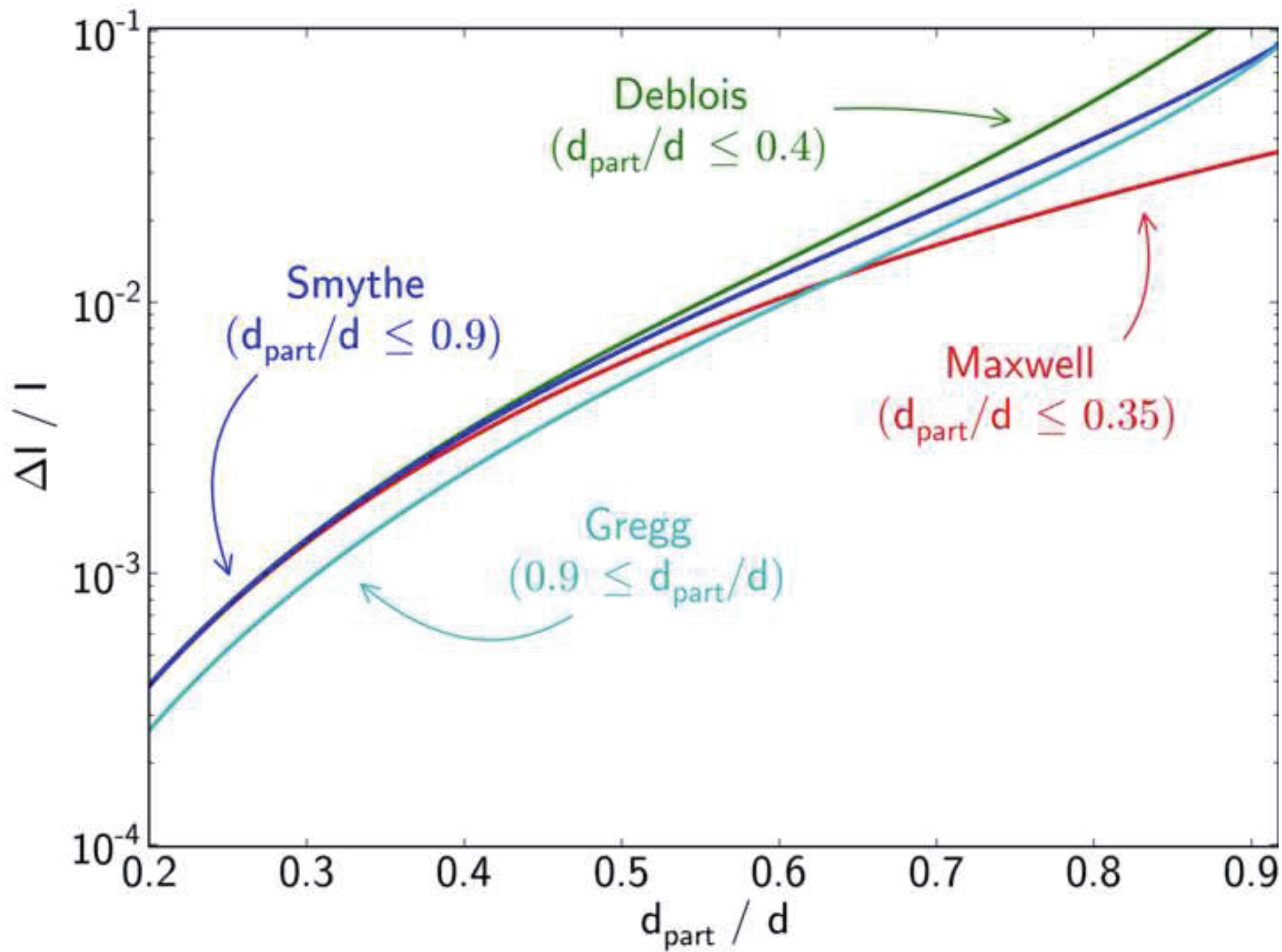


Figure 3
[Click here to download high resolution image](#)

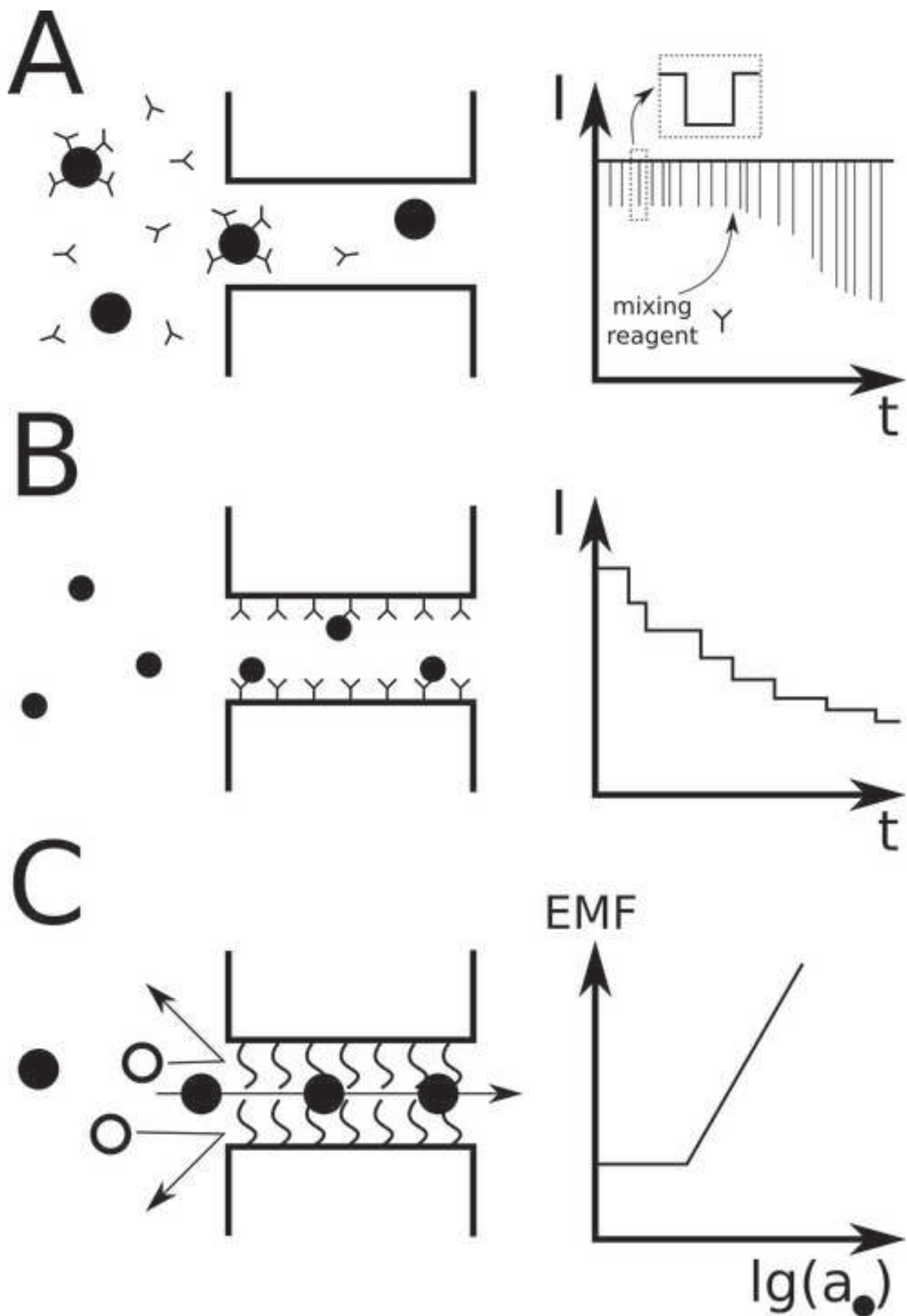


Figure 4

[Click here to download high resolution image](#)

